Enzyme-Assisted Polymer Film Degradation-Enabled Biomolecule Sensing with Poly (N-isopropylacrylamide)-Based Optical Devices

Wei Zhang, Menglian Wei, Wildemar S. P. Carvalho and Michael J. Serpe*

Department of Chemistry, University of Alberta, Edmonton, Alberta, Canada, T6G 2G2

Phone: (780) 492-5778 Email: serpe@ualberta.ca

Abstract

A biosensor for mouse Immunoglobulin G (IgG) was generated from responsive polymer-based interference filters (etalons). To accomplish this, an excess amount of alkaline phosphatase-modified goat anti-mouse IgG (AP-GAM, $F(ab')_2$ fragment specific to mouse IgG) was added to mouse IgG, and allowed to react for some time. After a given reaction time, the bound AP-GAM could be isolated from the unbound, excess AP-GAM by addition of goat anti-mouse IgG (Fc fragment specific)-modified magnetic microspheres (GAM-M) that bind the mouse IgG bound to AP-GAM. After application of a magnetic field, the free, unbound AP-GAM was isolated from the mixture and exposed to an etalon that has its upper Au surface modified with phosphate-containing polymer that can be degraded by AP-GAM. By the phosphate-containing polymer being degraded by the excess AP-GAM, the cleaved phosphate groups can diffuse into the interference filter's active polymer layer that yields a change in the optical properties that can be related to the amount of IgG in the sample. This concept is extremely straightforward to implement, and can be modified to detect a variety of other analytes of interest.

Key Words：Sensing, Biosensing，Poly (N-isopropylacrylamide), Etalons, Enzymatic

degradation

Pathogens, such as bacteria and viruses, are a major class of species that can have direct negative impacts on human and animal health. [1-3] Most recently, Zika virus has emerged as a major health concern in South America and other tropical areas around the world. Oftentimes, Zika virus infection has no symptoms, which makes it very difficult to diagnose. Therefore, those infected usually are not aware,[4] which can lead to extremely negative impacts on reproductive health.[5] As of 2016, there is no known cure for Zika virus, and no vaccine to prevent it. Therefore, an approach that can alert people when they are infected can help circumvent the negative impacts on those infected, especially to those that are, or are planning to become, pregnant.

Due to the high specificity of antibodies for particular epitopes on corresponding antigens, antibody-based detection systems for specific antigens have been used as versatile and powerful tools for bioanalysis.[6,7] Thus far, many biosensors have been developed, with one of the most commonly used approaches being enzyme-linked immunosorbent assay (ELISA) that exploits antibody-antigen interactions.[8,9] However, in many cases, ELISA requires significant time to perform, the surface chemistry needs to be carefully tuned for each specific analyte, and it requires a lab setting to achieve quantitative results. Lateral flow assays (LFA) for antibody/antigen detection have also attracted significant attention due to their ease of fabrication, the ability to use small sample volumes, while maintaining high quality figures of merit (e.g., high sensitivity and low detection limits). The most common and widely used LFA is the

home pregnancy test. Although LFAs are extremely useful, there are some issues with biomolecular affinities as the reaction times between the capture and analyte biomolecules is short and there is the possibility of non-specific reactivity to the LFA substrate. Much attention has also been focused on a variety of other approaches that exploit various phenomena, e.g., surface plasmon resonance (SPR),[10-12] quartz crystal microbalance (QCM),[13] and electrochemical impedance spectroscopy.[14] With these various approaches available, there is still a need for new cost-effective sensing technologies with high specificity and sensitivity, so that people, especially those in developing countries and low-income regions, will have disease diagnosis kits more readily available to them.

Recently, photonic materials/crystals have played important roles in various analytical and medical fields. [15-19] In 2010, the Serpe Group reported on a novel optical device (etalon) that can be fabricated by sandwiching a layer of poly (N-isopropylacrylamide) (pNIPAm)-based microgels between two thin, semi-transparent metal layers (typically Au in our case).[20] The structure of the microgel-based etalons is shown in Scheme 1. Briefly, etalons are fabricated by painting a concentrated solution of pNIPAm-based microgels onto a Au-coated glass substrate, followed by washing away the excess microgels that are not directly attached to the Au. Then the etalon is soaked in water and further rinsed before deposition of another Au layer on top of the microgels. The etalons show visible color and exhibit unique multipeak reflectance spectra. The position of the peaks and the peak order can be predicted by the equation (1):

$$\lambda m = 2nd \cos\theta \qquad (1)$$

where the specific wavelength maximum (λ) of a peak depends on the peak order (m), the refractive index of the dielectric (n) and the spacing between the mirrors (d), as well as the angle of incidence (θ). As a result, the size of the microgels is one factor that can dictate the color of the devices and the position of the devices reflectance peaks. We have used this structure for a variety of applications, primarily focused on sensing, biosensing and drug delivery. [21-25]

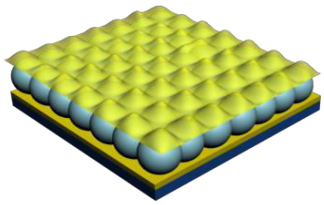

Scheme 1. The structure of a pNIPAm microgel-based etalon, which consists of two 15 nm Au mirrors (yellow layers), with 2 nm Cr adhesion layer. The mirrors sandwich a densely packed layer of microgels (blue layer) all assembled on a rigid glass substrate (dark bottom layer).

In this submission, a new sensing motif is introduced that utilizes positively charged pNIPAm-co-N-(3-Aminopropyl) methacrylamide hydrochloride (APMAH) microgel-based etalons coated with enzyme-responsive/reactive species to detect biomolecules; specifically mouse IgG in this submission. These experiments serve as a proof of concept for sensing other antigens in samples. As shown in Scheme 2, the immunoassay is performed by adding an excess amount of alkaline phosphatase-modified

goat anti-mouse IgG (AP-GAM) (F(ab')2 fragment specific to mouse IgG) to mouse IgG in solution, and allowing them to interact for 30 min. After 30 min, the AP-GAM was isolated from the unbound, excess AP-GAM via addition of goat anti-mouse IgG (Fc fragment specific)-modified magnetic microparticles (GAM@M). After application of a magnetic field, the free, unbound AP-GAM could be isolated and exposed to the etalon. The etalons here were coated with a phosphate-containing polymer that is cleaved by AP-GAM and releases phosphate. The released phosphates are then available to diffuse into the microgel layer where they neutralize the charges on the microgels, which yields a shift in the position of the peaks in the etalon's reflectance spectrum. Finally, the shift in the reflectance peak can be correlated to the initial concentration of mouse IgG. While we use a reflectance spectrometer to probe the optical properties of the devices in this investigation, we are moving toward generating a hand-held device containing simplified optics (or even the light source/camera from a cellular phone) to probe the optical properties of the devices to make the measurements truly portable.

To accomplish this, pNIPAm-co-APMAH microgels were synthesized and used to generate etalons according to previously published protocol.[26, 27] Briefly, NIPAm and APMAH were copolymerized at 70 ^{O}C, using ammonium persulfate (APS) as the initiator and N, N'-methylenebis(acrylamide) as the crosslinker. The approximate diameter of the prepared microgels was measured via dynamic light scattering (DLS) to be 1042 ± 9 nm. Transmission electron microscopy (TEM) was used to further

characterize the microgels, and a representative image can be seen in Figure 1. The resulting microgels were used to fabricate etalons as shown in the photograph in the insert of Figure 1. To generate the phosphate-containing polymer, phosphoric acid 2-hydroxyethyl methacrylate ester (chemical structure shown in Figure S1) was polymerized using APS as the initiator under N_2 atmosphere at 60 ^{O}C. Following synthesis, the polymer was purified via dialysis. The concentration of the solution after dialysis was 0.01 g/mL. The molecular weight of the synthesized polymer was measured by gel permeation chromatograph (GPC) to be 1.099×10^6 with a PDI 1.166. 200 μL of the polymer solution was then spin-coated onto the top layer of the etalon and allowed to dry. The spin-coating process was repeated another two times to make sure there was adequate polymer deposited on the top of Au surface. After deposition, the surface was rinsed with deionized water and soaked in PBS buffer solution. The thickness of resultant polymer layer was measured via ellipsometry to be 156 ± 4 nm. The deposition of the polymer layer is also evidenced by the XPS data (Figure S2 and Figure S3).

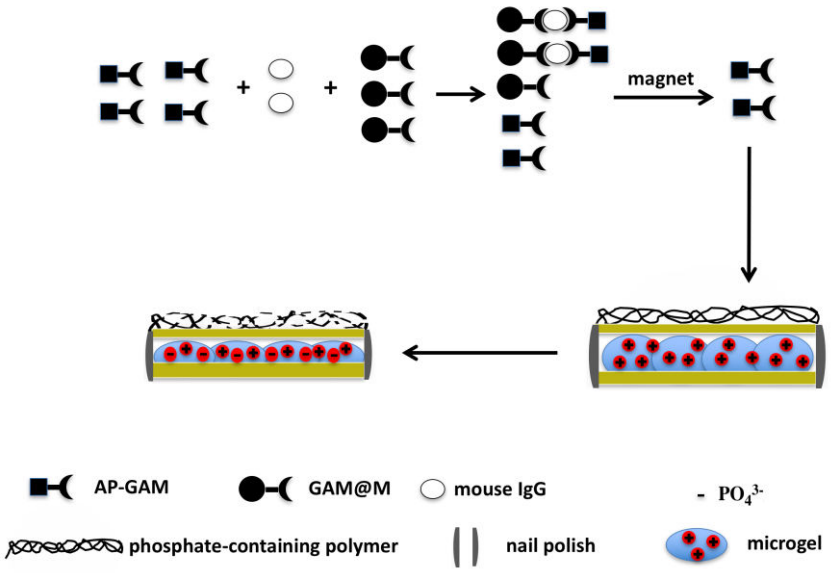

Scheme 2. Flow chart for how the immunoassay works.

To perform the assay, 150 μL of GAM@M suspension, 270 μL of PBS buffer solution, 1.7 μL (dissolved in 28 μL PBS buffer) of AP-GAM were added into six separate centrifuge tubes. Then into these tubes, was added 0 μg (0 pmol), 0.1 μg (0.67 pmol), 0.2 μg (1.34 pmol), 0.3 μg (2.01 pmol), 0.4 μg (2.68 pmol) and 0.5 μg (3.35 pmol) mouse IgG, respectively. Each tube was then wrapped in aluminum foil and gently shook for 1 h at 37 ℃. After 1 h, the magnetic beads were separated from the solutions by exposing each tube to an external magnet, which pulled the magnetic particles to the tube's inside wall. The supernatant solution was collected, which contained excess AP modified GAM. To ensure that all the excess AP modified GAM was collected, the magnetic beads were washed by adding 100 μL of PBS into the tube, mixing, magnetically separating the particles from the solution, and collecting the supernatant

solution. This process was completed a total of 3 times for each tube. Finally all the aliquots from each individual tube were combined, and used to react with the etalon. To confirm that all the magnetic beads were separated from the solution, we used dynamic light scattering (DLS) to measure the size of any particles in the solution. No particles with a diameter on the order of the magnetic particles used here (3.5 μm) were observed indicating that the magnetic particles were effectively removed from solution.

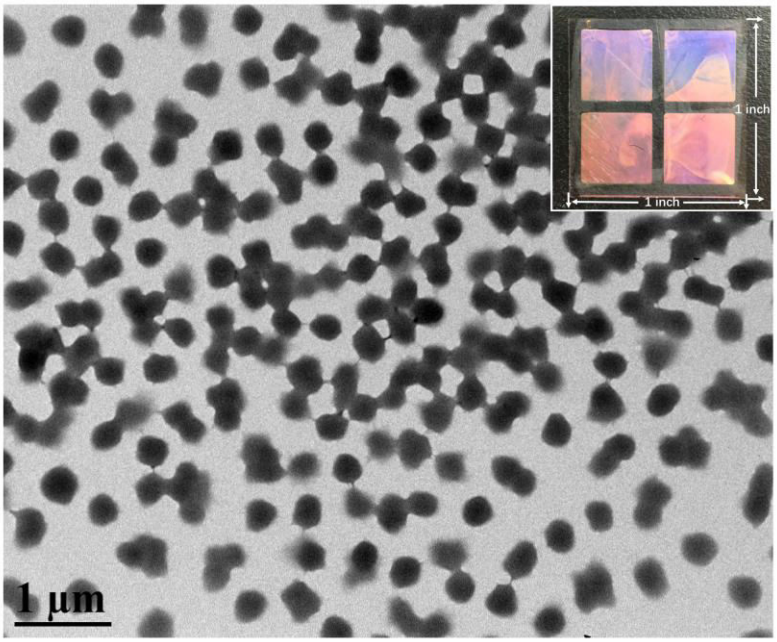

Figure 1. TEM image of the microgels. Insert is a photo of a representative etalon we used for performing the immunoassay.

Then on top of each individual etalon (0.375 inch × 0.375 inch), 100 μL PBS buffer was added to stabilize the etalon, followed by addition of 50 μL of the supernatant obtained from the reaction solutions described above. The etalon was placed on a hotplate,

with the temperature set at 37 ℃. Note that while the reaction can take place at room temperature, we used 37 ℃ to mimic the conditions found in the human body. After ~5 min, a blue shift of the reflectance peak was observed that stabilized within 30 min. The reflectance spectra were collected before and after (10 min, to minimize the reaction time but still obtain an adequate sensor response) addition of supernatant solution obtained from the reaction. Typical reflectance spectra of the etalon before and after exposure to AP-GAM solution are shown in Figure 2 (actual reflectance spectra for all experiments are shown in the electronic supporting information (ESI) Figure S4). The reflectance spectra collected at various times after exposure to AP-GAM are shown in Figure S5. We observed that in the initial ~4 min, the reflectance peaks shift slowly, stabilizing after ~10 min. Although, for practical applications, the total peak shift is only required to quantify the concentration of mouse IgG in solution. As can be seen from Figure 3, lower initial concentrations of the mouse IgG yield high concentrations of AP-modified GAM left in solution, which leads to larger shifts in the peak position.

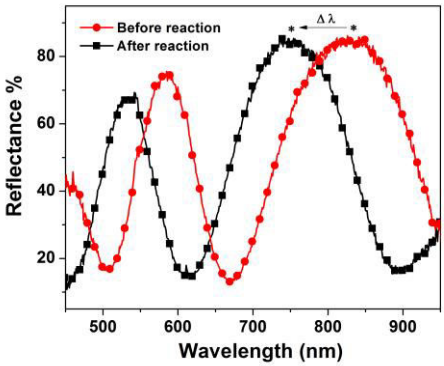

Figure 2. Reflectance spectra of the etalon before and after reacting with AP-GAM

solution. In this case, the AP-GAM solution was obtained after reaction with 0.1 μg mouse IgG (1.1 nM). The stars above the respective spectra indicate the position of the reflectance peaks before and after exposure of the etalon to excess AP-GAM.

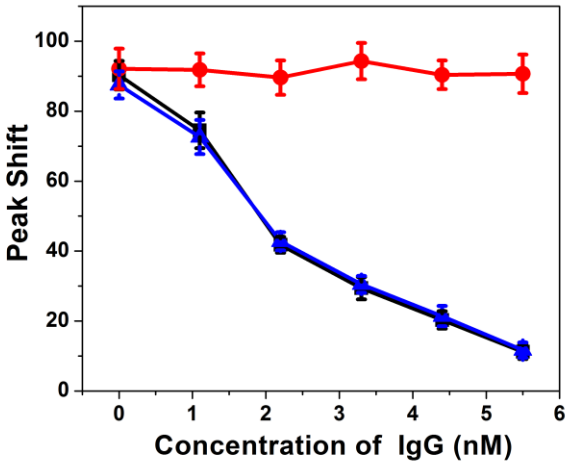

Figure 3. Peak shift of the reflectance spectrum from the etalon as a function of IgG concentration (■ for mouse IgG, ● for rabbit IgG and ▲ for mouse IgG in the presence of rabbit IgG). Each data point is the average obtained from three individual experiments, and the error bars are the standard deviations of the measured values. We point out that the lines drawn through the data in the plot are meant to guide the eye, and are not model fits to the data.

A proposed mechanism for the observed phenomenon is that the excess AP-GAM catalyzes the degradation of the phosphate-containing polymer layer on top of the etalon, which releases negatively charged phosphate moieties. These negative phosphate moieties are capable of penetrating the etalon's microgel layer and interacting with the positively charged APMAH cations on the microgels. Before this interaction, the

pNIPAm-co-APMAH microgels are positively charged and the positive charges tend to repel one another, which causes the microgel to exist in a swollen state. The accumulation of the negative phosphate ions around/inside the microgels will neutralize the APMAH cations and cause the pNIPAm-co-APMAH microgel to deswell. As can be seen from the reflectance spectra, a blue shift is observed, supporting the proposed mechanism. To further validate the proposed mechanism, we mixed 200 μL of the phosphate polymer solution with 20 mL PBS buffer and added 10 μL of the AP-GAM solution. As shown in Figure S1, the phosphate groups are part of the polymer network and are not fully charged in the polymer, because the oxygen atom within the phosphate group is covalently bound to the carbon atom. After reacting with AP-GAM, the small phosphate molecules with negative charges, such as monosodium phosphate and disodium phosphate, were released from the polymer network that should result in an increase in the conductivity of the solution. After reacting for 30 min at 37 ℃, we characterized the conductivity change of the solution. Before reaction the conductivity of the solution was 29.14 mS/cm (containing AP-GAM), after reaction, the conductivity increased to 30.20 mS/cm. This is evidence supporting our hypothesized mechanism above.

The selectivity of the assay was also determined by exposing AP-GAM and GAM@M to various amounts of rabbit IgG. Using the same approach as above for detecting mouse IgG, we isolated the remaining, unbound AP-GAM and used it to react with the etalon. As can be seen in Figure 3, there is almost no response of the system to

rabbit IgG, proving that the assay is specific for the mouse IgG. Finally, we showed that mouse IgG could be quantified in the presence of rabbit IgG. As can be seen in Figure 3, the quantification of mouse IgG is unaffected by the presence of rabbit IgG, suggesting that this assay can be a robust method for quantifying proteins in the presence of interfering species. Finally, to determine if the buffer for AP-GAM alone affects the response of the etalon, we added 2 μL of the buffer for AP-GAM to a PBS buffer stabilized etalon, no peak shift was observed (Figure S6).

In summary, we developed a novel immunoassay that utilized the cleavage of a polymer coated on the surface of a responsive polymer-based etalon to result in a change in its optical properties; the change in optical properties could be related to the amount of specific IgG in solution. We showed that the approach is specific, and can be effective in the presence of other interfering biomolecules in solution. This particular assay is simple and straightforward to carry out, and all the components are inexpensive, making this an assay that could find real world applications. While the devices here are specific to mouse IgG, the approach can be simply modified to detecting other antigens and biomolecules of interest, eventually leading to the detection of whole bacteria via antibody binding to specific biomolecules on the surface of bacteria and pathogens.

Acknowledgements

MJS acknowledges funding from the University of Alberta (the Department of Chemistry and the Faculty of Science), the Natural Sciences and Engineering Research Council of Canada (NSERC), the Canada Foundation for Innovation (CFI), the Alberta Advanced Education & Technology Small Equipment Grants Program (AET/SEGP), Grand Challenges Canada and IC-IMPACTS. MJS also thanks Prof. Chris Cairo for helpful discussions.

References

(1) Walsh, T. R.; Weeks, J.; Livermore, D. M.; Toleman, M. A. *Lancet Infect. Dis.* **2011**, *11*, 355-362.

(2) Lundberg, J. O.; Weitzberg, E.; Cole, J. A.; Benjamin, N. *Nature Rev. Microbiol.* **2004**, *2*, 593-602.

(3) Peiris, J. M.; De Jong, M. D.; Guan, Y. *Clin. Microbiol. Rev.* **2007**, *20*, 243-267.

(4) Duffy, M. R.; Chen, T.-H.; Hancock, W. T.; Powers, A. M.; Kool, J. L.; Lanciotti, R. S.; Pretrick, M.; Marfel, M.; Holzbauer, S.; Dubray, C. *N. Engl. J. Med.* **2009**, *360*, 2536-2543.

(5) Brasil, P.; Pereira, J., Jose P; Raja Gabaglia, C.; Damasceno, L.; Wakimoto, M.; Ribeiro Nogueira, R. M.; Carvalho de Sequeira, P.; Machado Siqueira, A.; Abreu de Carvalho, L. M.; Cotrim da Cunha, D. *N. Engl. J. Med.* **2016**,375, 2321-2334.

(6) Holford, T. R.; Davis, F.; Higson, S. P. *Biosens. Bioelectron.* **2012**, *34*, 12-24.

(7) Lanciotti, R. S.; Kosoy, O. L.; Laven, J. J.; Velez, J. O.; Lambert, A. J.; Johnson, A. J.; Stanfield, S. M.; Duffy, M. R. *Emerg. Infect. Dis.* **2008**, *14*, 1232-1239.

(8) Liu, B.H.; Tsao, Z.J.; Wang, J.J.; Yu, F.Y. *Anal. Chem.* **2008**, *80*, 7029-7035.

(9) Lee, P.; Plavina, T.; Castro, A.; Berman, M.; Jaiswal, D.; Rivas, S.; Schlain, B.; Subramanyam, M. *J. Clin. Virol.* **2013**, *57*, 141-146.

(10) Tran, D. T.; Knez, K.; Janssen, K. P.; Pollet, J.; Spasic, D.; Lammertyn, J. *Biosens. Bioelectron.* **2013**, *43*, 245-251.

(11) Breault Turcot, J.; Chaurand, P.; Masson, J.F. *Anal. Chem.* **2014**, *86*, 9612-9619.

(12) de Juan-Franco, E.; Caruz, A.; Pedrajas, J.; Lechuga, L. M. *Analyst* **2013**, *138*, 2023-2031.

(13) Cooper, M. A.; Singleton, V. T. *J. Mol. Recognit.* **2007**, *20*, 154-184.

(14) Lisdat, F.; Schäfer, D. *Anal. Bioanal. Chem.* **2008**, *391*, 1555.

(15) Satapathy, S. S.; Bho, P.; Aswathy, C.; Mohanta, J.; Samantaray, K.; Bhat, S. K.; Panda, S. K.; Mohanty, P. S.; Si, S. Applied Surface Science 2017.

(16) Zhang, W.; Jiang, P.; Chen, J.; Zhu, C.; Mao, Z.; Gao, C. *J. Colloid Interface. Sci.* **2017**, 490, 181-189.

(17) Elashnikov, R.; Mares, D.; Podzimek, T.; Švorčík, V.; Lyutakov, O. Analyst **2017**, 142, 2974-2981.

(18) Wang, T.; Yu, Y.; Chen, D.; Wang, S.; Zhang, X.; Li, Y.; Zhang, J.; Fu, Y. Nanoscale **2017**, 9, 1925-1933.

(19) Wang, Z.; Zhang, J.; Wang, Z.; Shen, H.; Xie, J.; Li, Y.; Lin, L.; Yang, B. J. Mater. Chem. C **2013**, 1, 977-983.

(20) Sorrell, C. D.; Serpe, M. J. *Adv. Mater.* **2011**, *23*, 4088-4092.

(21) Islam, M. R.; Lu, Z.; Li, X.; Sarker, A. K.; Hu, L.; Choi, P.; Li, X.; Hakobyan, N.; Serpe, M. J. *Anal. Chim. Acta* **2013**, *789*, 17-32.

(22) Gao, Y.; Li, X.; Serpe, M. J. *RSC Adv.* **2015**, *5*, 44074-44087.

(23) Islam, M. R.; Gao, Y.; Li, X.; Zhang, Q. M.; Wei, M.; Serpe, M. J. *Chin. Sci. Bull.* **2014**, *59*, 4237-4255.

(24) Zhang, W.; Guo, S.; Carvalho, W. S. P.; Jiang, Y.; Serpe, M. J. *Anal. Methods* **2016**, *8*, 7847-7867.

(25) Gao, Y.; Ahiabu, A.; Serpe, M. J. *ACS Appl. Mater. Interfaces* **2014**, *6*, 13749-13756.

(26) Islam, M. R.; Serpe, M. J. *Anal. Chim. Acta* **2014**, *843*, 83-88.

(27) Islam, M. R.; Serpe, M. J. *Anal. Bioanal. Chem.* **2014**, *406*, 4777-4783.